JOURNAL OF CATALYSIS 177, 175–188 (1998)
ARTICLE NO. CA982048

Electronic Effects and Effects of Particle Morphology in n-Hexane Conversion over Zeolite-Supported Platinum Catalysts

Paul V. Menacherry* and Gary L. Haller†

Department of Chemical Engineering, Yale University, New Haven, Connecticut 06520

Received January 6, 1997; revised January 29, 1998; accepted February 23, 1998

n-Hexane conversion over zeolite-supported platinum catalysts has been studied at 360°C in a packed bed reactor. In the absence of sulfur impurities, the deactivation appears to be due to two types of coke formation. The propensity for terminal hydrogenolysis is primarily determined by the particle morphology, i.e., the type of surface sites exposed. The increase in benzene selectivity correlates with a shift to lower stretching frequencies of the CO absorption bands, indicating that an increase in the electron density at the surface metal atoms results in higher benzene selectivity. The effect of the support in the high activity and aromatization selectivity of a monofunctional platinum catalyst for n-hexane conversion is observed to be twofold, i.e., the stabilization of extremely small metal particles of specific morphology under reaction conditions and metal–support interaction, resulting in an increased electron density over the metal particles. © 1998 Academic Press

INTRODUCTION

Since the initial report by Bernard (1) about the remarkable aromatization properties of small platinum clusters in nonacidic L-zeolite, different hypotheses have been put forward to explain the high aromatization selectivity of these catalysts (2–6). Tauster and Steger (2) correlated high benzene selectivity with the propensity for terminal hydrogenolysis and proposed that the linear channels of the L-zeolite favor n-hexane adsorption at the terminal carbon atom, leading to increased benzene formation. Derouane and Vanderveken (3), based on molecular simulations of the van der Waals interactions between n-hexane molecules and the L-zeolite pore walls, proposed that the high benzene selectivity was due to the preorganization of the n-hexane molecule as a pseudocycle leading to (1, 6) ring closure. However, subsequent research showed that comparable benzene selectivities could be obtained over platinum supported on magnesia (7), in which no such preorganization/collimating effects can be expected. Mielczarski *et al.* (4) observed that the correlations between the high benzene selectivity and terminal cracking can be extended to platinum supported on faujasite, silica, and microporous carbon, and concluded that the high aromatization selectivities observed over monofunctional platinum catalysts are independent of support microporosity. Iglesia and Baumgartner (5) reported that both Pt/K L-zeolite and Pt/silica have comparable initial selectivities for aromatization, but the inhibited deactivation of the former retains the intrinsic activity and selectivity, while the deactivation caused by coking on the Pt/silica decreases both the activity and aromatic selectivity of these catalysts. A similar conclusion was reached by Sharma *et al.* (6) based on microcalorimetric and C^{13} NMR studies of CO adsorption before and after n-hexane conversion over Pt/BaK L-zeolite and Pt/silica catalysts. These studies (4–6) suggest that the high propensity for terminal adsorption, which correlates with the aromatization selectivity, is an intrinsic function of clean platinum surfaces. Paal and coworkers (8–12) have studied n-hexane conversion in a closed loop recirculation reactor system, at temperatures (~603 K) much lower than in typical reforming conditions and subatmospheric pressures. Under these conditions, methylcyclopentane (MCP) and methylpentanes (MP) are the major products, and the benzene selectivity is usually less than 30% for most samples. Paal (13, 14) has proposed that the ratio of MCP to MP is a measure of the abundance of surface hydrogen, with lower concentrations of surface hydrogen leading to a higher MCP to MP ratio. Therefore, higher MCP to MP ratios can be expected to correlate with increased benzene selectivity (13, 14). Although interesting correlations such as the increased benzene selectivity with increase in the terminal cracking (2, 4), inhibited deactivation of the catalysts (5, 6), and increase in the MCP to MP ratio (13, 14) have been proposed, n-hexane conversion over monofunctional platinum catalysts is still not completely understood due to the interplay of both electronic and geometric effects. In the present study we have investigated deactivation profiles for n-hexane conversion over zeolite supported platinum in a packed bed reactor configuration under reaction conditions similar to that used in the studies by Paal and co-workers (8–12).

* Present address: Precision Combustion, Inc., 25 Science Park, New Haven, CT 06511.

† Corresponding author. Telephone: (203) 432-4378; Fax: (203) 432-4387. E-mail: gary.haller@yale.edu.

0021-9517/98 $25.00

Electronic effects and effects of particle morphology in these catalysts were probed using the infrared absorption of carbon monoxide (CO) adsorbed on the metal particles.

The CO stretching frequency is an excellent indicator of the manner in which the CO molecule is bound to the substrate, and this technique has been extensively used to characterize supported metal catalysts (15–21). The different absorption bands for CO adsorbed on transition metal surfaces have been classified as follows (15). Absorption bands between 2130 and 2000 cm^{-1} have been assigned to linearly adsorbed CO species, bands between 2000 and 1880 cm^{-1} to twofold or bridging species, and bands between 1880 and 1650 cm^{-1} to CO adsorbed on multicenter adsorption sites. In the generally accepted view of CO chemisorption on transition metals (22, 23), the CO is coordinatively bonded to the metal atom via the 5σ orbital, and the d orbitals of the metal atom backdonate charge to the $2\pi^*$ orbital, which is M–C bonding and C–O anti-bonding. An increase in the electron density of the metal d orbitals results in an increased occupation of the $2\pi^*$ orbital, weakening the C–O bond. This can be observed in the infrared of adsorbed CO as a shift of the CO absorption bands to lower frequencies. Also, van Santen (24) has recently proposed that an increase in electron density leads to an increase in the bridged to linear adsorbed CO species. The CO stretching frequency can therefore be used to probe the electron density on the adsorbing metal atoms. However two types of electronic effects need to be distinguished. An electronic perturbation of the metal particles can result from a charge transfer to or from the support. For example, in recent research in our laboratory, we observed that the addition of trace amounts of water results in a shift to lower frequencies of the CO absorption bands, which we interpreted as an increase in the electron density of the metal particles, resulting from a perturbation of the metal–support interaction (25). A second type of electronic effect is related to the morphology of the metal particles and the structure of the metal surface exposed. Surface atoms have an incomplete set of next nearest neighbor metal atoms. Blyholder's model (26) predicts that the more coordinatively unsaturated the adsorbing metal atom (i.e., the less the number of nearest neighbor metal atoms) the lower will be the CO stretching frequency. Greenler *et al.* (27) have correlated the CO stretching frequencies on a series of Pt/silica catalysts having different average particle sizes with the relative number of face, corner and edge atoms (C_9^3, C_7^5, and C_6^6, in the notation of van Harteveld and Hartog (28) calculated for the average particle size. More recently, Kappers and van der Maas (29) have proposed a correlation between the linear CO stretching frequencies and the metal coordination number of the adsorbing atom. Therefore, the infrared of adsorbed CO is a sensitive probe of both electronic effects and effects of particle morphology. One drawback of this technique is the dipole-dipole coupling between the adsorbed CO molecules, first reported by Eischens *et al.* (30), and recently reviewed by Hollins and Pritchard (31, 32). Dipolar coupling can result in shifts to higher frequencies, changes in the molecular absorption coefficients of the adsorbed species, and intensity transfers from lower frequency bands to higher frequency bands (31, 32), and this can complicate the interpretation of the infrared spectra. In the present study, we have subjected saturation uptakes of CO at room temperature (RT) to equilibration at different temperatures (100, 200, and 300°C) in an inert gas. This treatment results in both a redistribution and a net desorption of adsorbed CO, and in this way the coverage dependence of CO stretching frequencies has been studied over these catalysts. The CO infrared experiments have been used to probe both the electronic state and the surface sites exposed for CO adsorption over our zeolite supported Pt catalysts. We have attempted to correlate the results of the n-hexane conversion studies with the CO infrared studies to distinguish between electronic effects and effects of particle morphology for n-hexane conversion over these catalysts.

EXPERIMENTAL

Catalyst Preparation

The catalysts used in this study and their hydrogen chemisorption uptakes (extrapolated to zero pressure) are reported in Table 1. The BaKL-zeolite support was prepared by ion-exchanging the Ba^{2+} into K L-zeolite and calcining to induce ion migration to the locked cages, prior to metal loading. Platinum was incorporated by ion-exchange (IE) using tetraamine platinum nitrate precursor. In two of the samples, the Brønsted acidity generated upon reduction of the ion-exchanged precursor was back-exchanged (BE) with K^+. Infrared absorption spectra of the hydroxyl stretching region (reported elsewhere (33)) confirms that the back-exchange was successful in exchanging all of the Brønsted acidity. Furthermore, a comparison of the X-ray absorption fine structure (XAFS) chi functions of the ion-exchanged and the back-exchanged samples indicates that the particle morphology remains unchanged upon back-exchange of the protons for K^+ (33). First shell coordination numbers determined from XAFS are ~5 for the 3.67 wt%

TABLE 1

Hydrogen Chemisorption Uptakes (H/M)

Catalyst	H/M
Pt/BaKL-(5.5 wt%)	1.19
Pt/KL-(5.5 wt%)	1.12
Pt/KL-(3.67 wt%)	1.71
Pt/KL-(3.67 wt%, BE)	1.61
Pt/KY-(3.67 wt%)	1.34
Pt/KY-(3.67 wt%, BE)	1.14

Pt/L-zeolite samples and ~6 for the 5.5 wt% Pt/BaKL and the 3.67 wt% Pt/Y-zeolite samples (34), indicating the formation of very small metal particles. Calculations of the variation of XAFS coordination numbers with particle size for different particle morphologies (34) indicates an average particle size for the 3.67 wt% Pt/L-zeolite samples of ~12 atoms and for the 5.5 wt% Pt/BaKL and the 3.67 wt% Pt/Y-zeolite samples of ~18 atoms. This is consistent with the hydrogen chemisorption results (H/M > 1). Details of the catalysts preparation and hydrogen uptake measurements have been reported elsewhere (33, 35).

CO Infrared Studies

A 1000 ppm CO in helium blend was obtained from Scott Specialty Gases. This was further purified using a 5A molecular sieve trap (Supelco) to remove trace CO_2 and water impurities. Ultra high purity hydrogen and helium were further purified by an Oxysorb purifying trap (Supelco) and an OMI-2 indicating-purifying trap (Supelco). The controlled atmosphere infrared cell was equipped with CaF_2 windows and was capable of *in-situ* heating and cooling of the sample. The catalyst samples (~20 mg) were pressed into 13-mm diameter self-supported wafers before loading in the infrared cell. Transmission infrared spectra of adsorbed CO were acquired on a MIDAC M-series Fourier transform infrared (FTIR) spectrometer at a resolution of 2 cm^{-1}, by coadding 256 scans (~10 min total scan time).

The samples were heated to 400°C and rereduced at this temperature for 30 min under flowing hydrogen (40 cc/min). The flow was then switched to helium (40 cc/min) and the cell was purged with helium for 1 h at 400°C before cooling to RT. The flow was then switched to the CO/He blend (40 cc/min) until saturation uptake was reached (<30 min) and the infrared spectrum was obtained in the CO atmosphere. The flow was then switched to helium and the CO adsorption spectrum was obtained after a 30-min purge (at RT) in helium. Following this, the adsorbed CO was equilibrated at 100°C in an inert gas (helium). The catalyst was heated to 100°C (at 5 K/min) and maintained at this temperature for 30 min in flowing helium. The catalyst was then cooled to RT and the infrared spectrum of the undesorbed/redistributed CO was obtained. The flow was then switched to the CO/He blend and the infrared spectrum of the saturated CO uptake was obtained to check that the metal particles were unaffected by this treatment. This procedure was repeated for equilibration temperatures of 200 and 300°C. Peak positions were determined using the second derivatives technique described by Kappers and van der Maas (29). Second-order derivatives were calculated using a 15-point Savitzky–Golay derivative function (36).

n-Hexane Conversion

A 1.06% (by volume) blend of n-hexane in ultra high purity (UHP) helium was obtained from Matheson Gases. This was further purified using an OMI-2 indicating–purifying trap (Supelco) to remove trace impurities, especially sulfur-containing compounds. Ultra high purity hydrogen (Connecticut Airgas) was further purified using an Oxiclear purifying trap (Labclear Inc.) and an OMI-2 indicating–purifying trap (Supelco). The gas flow rates used were 42 cc/min for the n-hexane/He blend and 8 cc/min for hydrogen, corresponding to partial pressures of 7 and 125 Torr of n-hexane and hydrogen, respectively. The gases were premixed and passed through a preheating bed of α-alumina before reaching the catalyst bed. The reaction was carried out at atmospheric pressure in 4 mm ID Pyrex reactors in a packed bed configuration. The products were analyzed using an on-line gas chromatograph (Varian 3700) equipped with a flame ionization detector and a 30 ft, 23% SP™-1700 on 80/100 Chromosorb PAW support column (Supelco), which was unable to separate the lower (C_2 and C_3) alkenes from the corresponding alkanes, but which otherwise gave adequate resolution of the products.

Between 10 and 80 mg of sample (adjusted to have an initial n-hexane conversion of ~40%) was diluted in α-alumina to 200 mg. The catalyst was heated to 400°C, rereduced at this temperature for 30 minutes and then cooled to the reaction temperature (360°C) in 8 cc/min flow of hydrogen. After the reactor was stabilized at the reaction temperature, the n-hexane/He blend (42 cc/min) was admitted. The product stream was sampled after 10 min on-stream and then subsequently every 50 min for 5 h, and the catalyst deactivation was followed.

RESULTS

CO Infrared Studies

The absorption spectrum of the saturation CO uptake at RT following the highest temperature treatment (300°C) is identical to that after initial adsorption of CO at RT, confirming that the metal particle dispersions are not affected by the heating of the samples to these higher temperatures in an inert gas. The infrared absorption spectrum after saturation uptake obtained in the CO atmosphere is almost identical to that after a 30-min purge in helium, indicating that the CO is strongly chemisorbed on the metal particles. Figures 1a–f show the infrared absorption spectra of CO adsorbed at RT (saturation uptake followed by 30 min helium purge) and after equilibrating the CO (saturated uptake at RT) at higher temperatures in flowing helium for the different catalysts. Peak positions of the different CO absorption bands, corresponding to different adsorbed CO species, were determined using second derivatives of the absorption spectra (29). These are reported in Table 2. Equilibration of saturated uptakes (at RT) of CO at higher temperatures in helium resulted in both a redistribution and a net desorption of adsorbed CO. In particular, equilibration at the intermediate temperatures (100 and 200°C)

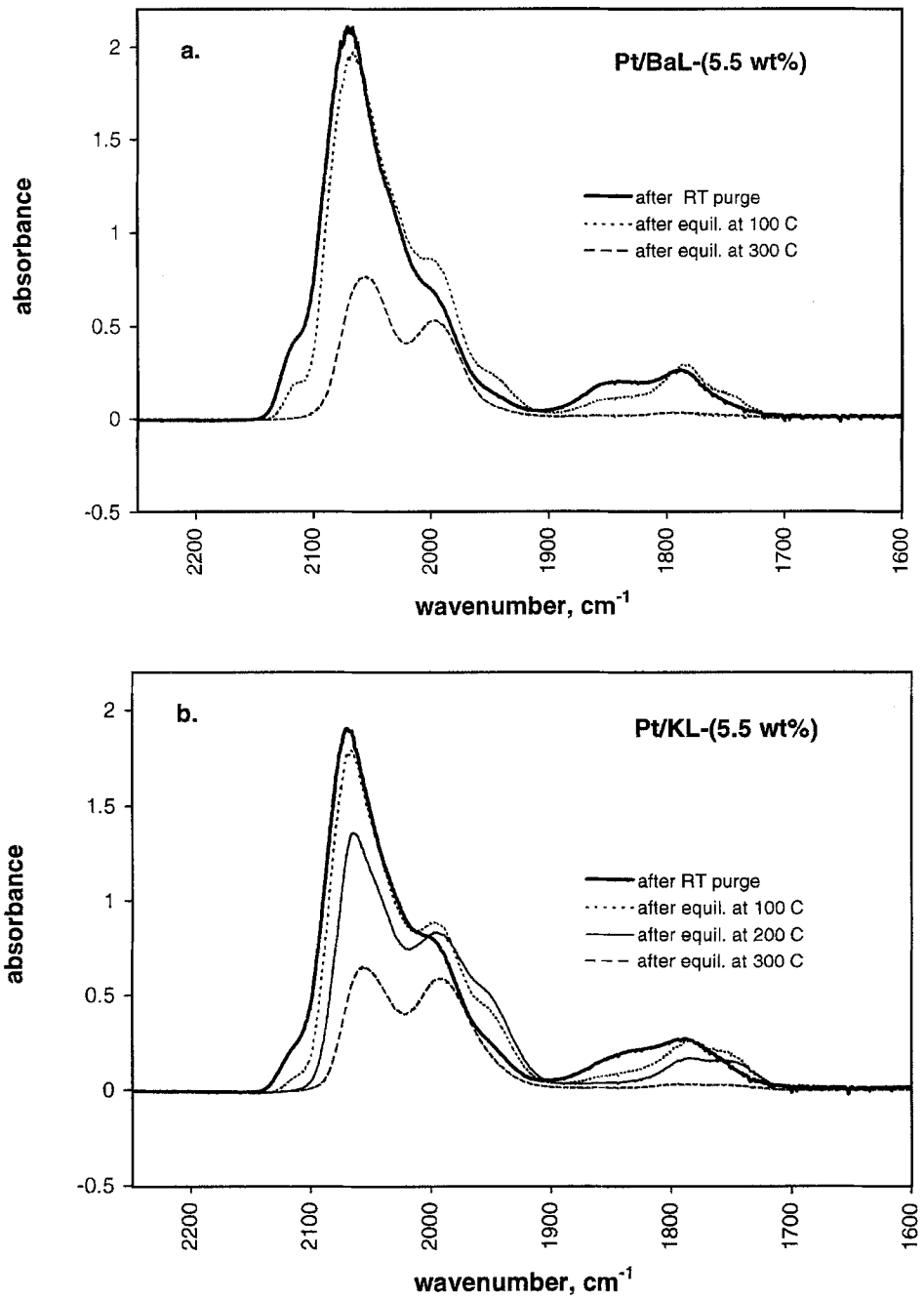

FIG. 1. CO absorption spectra after helium purge at RT and after equilibrating RT saturation uptakes of CO at higher temperatures in inert gas (helium) flow: a. Pt/BaL-(5.5 wt%); b. Pt/KL-(5.5 wt%); c. Pt/KL-(3.67 wt%); d. Pt/KL-(3.67 wt%, BE); e. Pt/KY-(3.67 wt%); f. Pt/KY-(3.67 wt%, BE).

results in an increase in the intensity of the absorption bands at ~1992 and 1946 cm^{-1}. This indicates an activation energy barrier to the adsorption of these species. From Table 2, it is seen that the absorption bands corresponding to linearly adsorbed CO are shifted to lower frequencies upon equilibration at higher temperatures, because of reduced dipole–dipole coupling effects, as a result of the net desorption of CO. The absorption spectra after equilibration at 300°C in helium are compared in Fig. 2.

n-Hexane Conversion

The conversion of n-hexane reactant and the turnover frequencies (TOF), normalized to the hydrogen chemisorption uptakes in Table 1, have been plotted against the time-on-stream (TOS) in Figs. 3a and 3b, respectively, for the different samples. From these figures it can be seen that the catalyst samples deactivate under the reaction conditions used. Zeolite-supported platinum catalysts are extremely

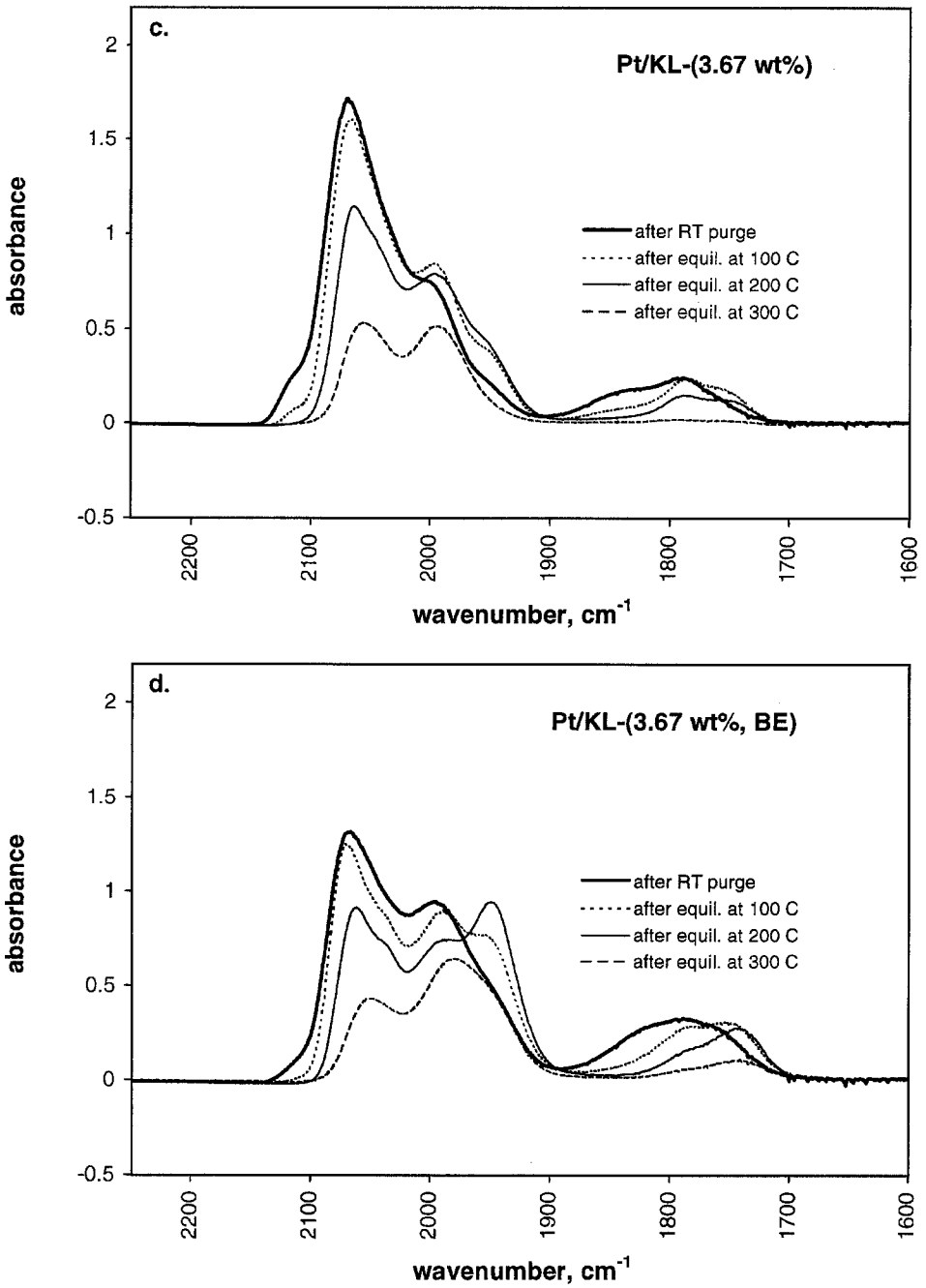

FIG. 1—*Continued*

sensitive to any sulfur compounds in the feed (37, 38). However, since any trace sulfur impurities would have been removed by the on-line traps, the deactivation in this case can be ascribed entirely to coking.

Figures 4a–h plot the selectivities (wt%) to different products versus TOS for the different samples. It is observed that after an initial period (~100 min TOS) these selectivities remain almost unchanged, except in the case of the hexene product (Fig. 4h), where the selectivity is seen to increase with TOS. The ratio of hexenes to n-hexane is plotted in Fig. 5. It is observed that the ratio of hexenes to n-hexane remain almost constant for the different samples, suggesting that the hexenes in the product stream are thermodynamically equilibrated. Indeed, the equilibrium constant for n-hexane dehydrogenation to 1-hexene (calculated using TAPP Version 2.2, EMS Software Inc.) is $K_c = 3.21 \times 10^{-3}$, which gives a hexene to n-hexane ratio of 0.02 for a hydrogen partial pressure of 0.16 (corresponding to the inlet flowrate of hydrogen), and the lower hexene to hexane ratio observed for the samples having higher

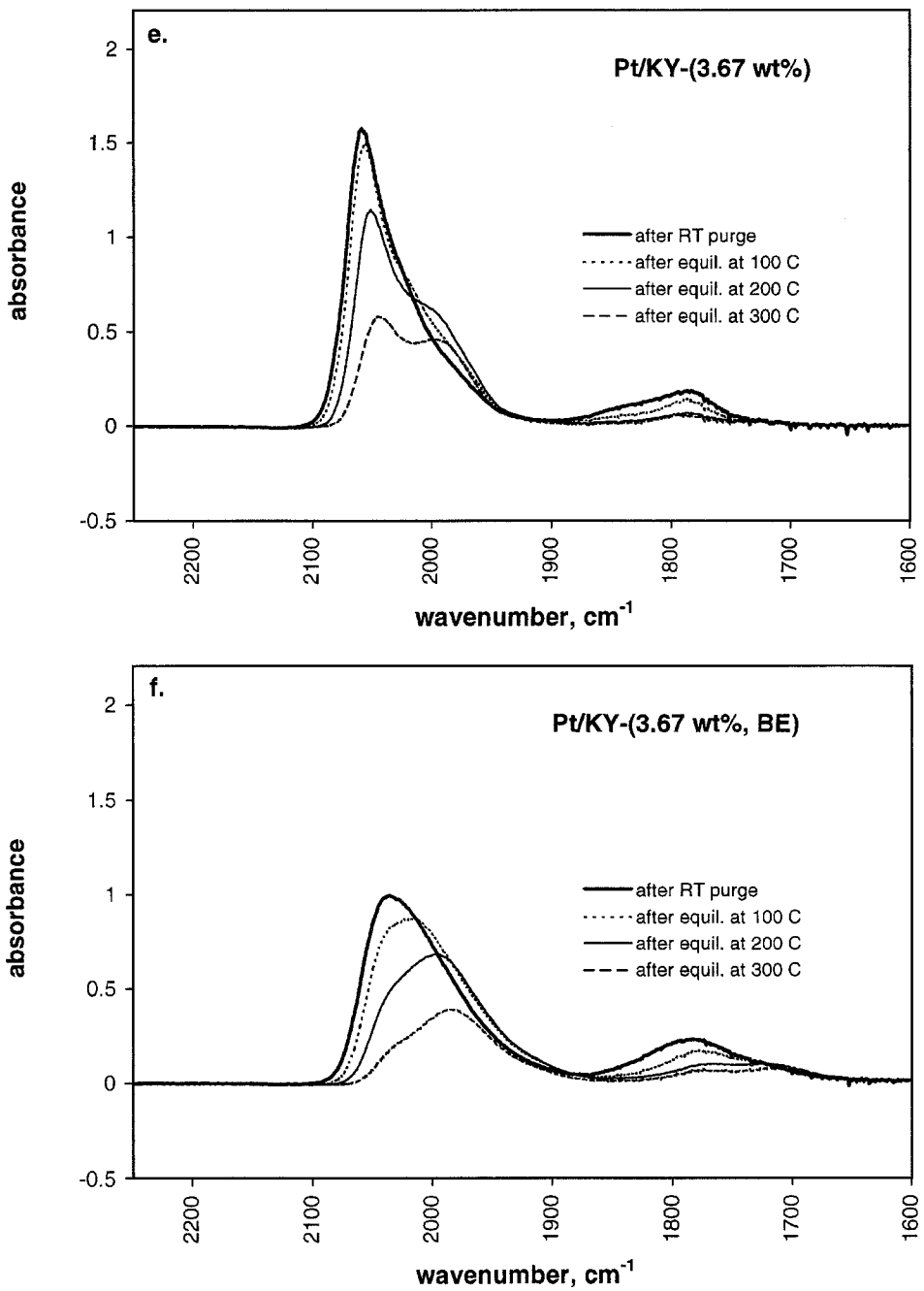

FIG. 1—*Continued*

benzene selectivity is consistent with the expected increase in the partial pressure of hydrogen upon dehydrogenation of n-hexane to benzene.

Product distribution patterns, i.e., the ratio of n-pentane to the sum of propane, n-butane, and n-pentane, i.e., n-C_5/(C_3 + n-C_4 + n-C_5), the MCP to MCP plus isomer ratio, i.e., MCP/(MCP + MP), the 2MP to 3MP ratio, and the ratio of benzene to C_5 cyclization products are plotted against the TOS in Fig. 6. Benzene selectivities over the different catalysts were observed to correlate with the infrared stretching frequency of linearly adsorbed CO (at the lowest coverages, i.e., after equilibration at 300°C in helium). This is shown in Fig. 7.

DISCUSSION

CO Infrared Studies

From Figs. 1a, 1b, and 1c and Table 2 it can be seen that the Pt/BaKL-(5.5 wt%), Pt/KL-(5.5 wt%), and Pt/KL-

TABLE 2

Peak Positions Determined by Second Derivatives Technique (29)

Catalyst	Peak positions, cm^{-1}							
Pt/BaKL-(5.5 wt%)								
RT	2122	2074	—	1993	—	1856	1786	—
100°C	(2120)	2074	—	1993	1943	1858	1786	1744
300°C	—	2064	—	1994	—	—	—	—
Pt/KL-(5.5 wt%)								
RT	(2121)	2074	—	1994	—	1855	1787	—
100°C	—	2072	—	1992	1947	(1857)	1787	1748
200°C	—	2068	—	1992	1948	—	1788	1744
300°C	—	2061	—	1992	—	—	—	—
Pt/KL-(3.67 wt%)								
RT	(2121)	2075	—	1994	—	1847	1788	—
100°C	—	2073	—	1993	1948	—	1789	1749
200°C	—	2069	—	1993	1948	—	1791	1745
300°C	—	2062	—	1993	—	—	—	—
Pt/KL-(3.67 wt%, BE)								
RT	—	2075	—	1992	1943	1825	1787	1758
100°C	—	2075	—	1992	1946	—	1787	1745
200°C	—	2067	2037	1994	1946	—	1788	1739
300°C	—	2056	2037	1985	1945	—	1788	1739
Pt/KY-(3.67 wt%)								
RT	—	2061	—	—	—	—	1782	—
100°C	—	2059	—	—	—	—	1785	—
200°C	—	2054	—	1994	—	—	1785	—
300°C	—	2048	—	1989	—	—	1786	—
Pt/KY-(3.67 wt%, BE)								
RT	—	2046	(2012)	—	—	—	1781	—
100°C	—	2044	2012	—	—	—	1780	—
200°C	—	2040	—	1992	—	—	1779	1711
300°C	—	2035	—	1984	—	—	1780	1707

(3.67 wt%) samples have very similar CO absorption bands, suggesting that the surface sites for the adsorption of CO are very similar over these catalysts (even though the hydrogen chemisorption uptakes would suggest different morphologies for the 5.5 and 3.67 wt% Pt/K L-zeolite samples). The absorption spectra are quite different for the Pt/KY-(3.67 wt%) catalyst (Fig. 1e). This indicates that the morphology of the metal particles formed is strongly influenced by the zeolite pore structure. Comparing the Pt/KL-(3.67 wt%) and Pt/KL-(3.67 wt%, BE) samples (Figs. 1c, 1d, and Table 2), it is seen that the back-exchange causes a shift of the CO absorption bands to lower frequencies. A comparison of the XAFS chi functions of the ion-exchanged and back-exchanged samples indicates that the back-exchange procedure does not affect the particle morphology for either the Pt/KL and the Pt/KY catalysts (33). Therefore, the shift in the absorption bands to lower frequencies is attributed to an increase in the electron density of the metal particles. This interpretation is in keeping with the observed increase in bridged to linear CO species, as suggested by van Santen (24). The CO absorption bands over Pt/K Y-zeolite sample are at lower frequencies compared to the Pt/L-zeolite samples. Platinum supported on Y-zeolite has previously been reported to be electron deficient (39, 40). Also Y-zeolite is generally believed to be more acidic (electron withdrawing) than L-zeolite. Therefore it is unlikely that charge transfer from the zeolite support to the metal particle can account for the increased electron density of the metal particles in Pt/Y-zeolite samples compared to the Pt/L-zeolite samples. A more likely explanation is that the morphology of the metal particles formed has more coordinatively unsaturated surface atoms. The Pt/KY back-exchanged sample shows a shift to lower frequencies and an increased ratio of bridged to linear CO species compared to the Pt/KY-(3.67 wt%) sample (Fig. 2b), consistent with an increase in the electron density of the metal particles upon back-exchanging the protons for K^+. From the position of the CO absorption bands after equilibration at 300°C (Figs. 2a and 2b), the order of increasing electron density of the surface sites exposed was determined as Pt/BaKL-(5.5 wt%) < Pt/KL-(3.67 wt%) < Pt/KL-(3.67 wt%, BE) < Pt/KY-(3.67 wt%) < Pt/KY-(3.67 wt%, BE). The first shell coordination numbers determined from XAFS spectroscopy (34) are about 5 for the 3.67 wt% Pt/K L-zeolite

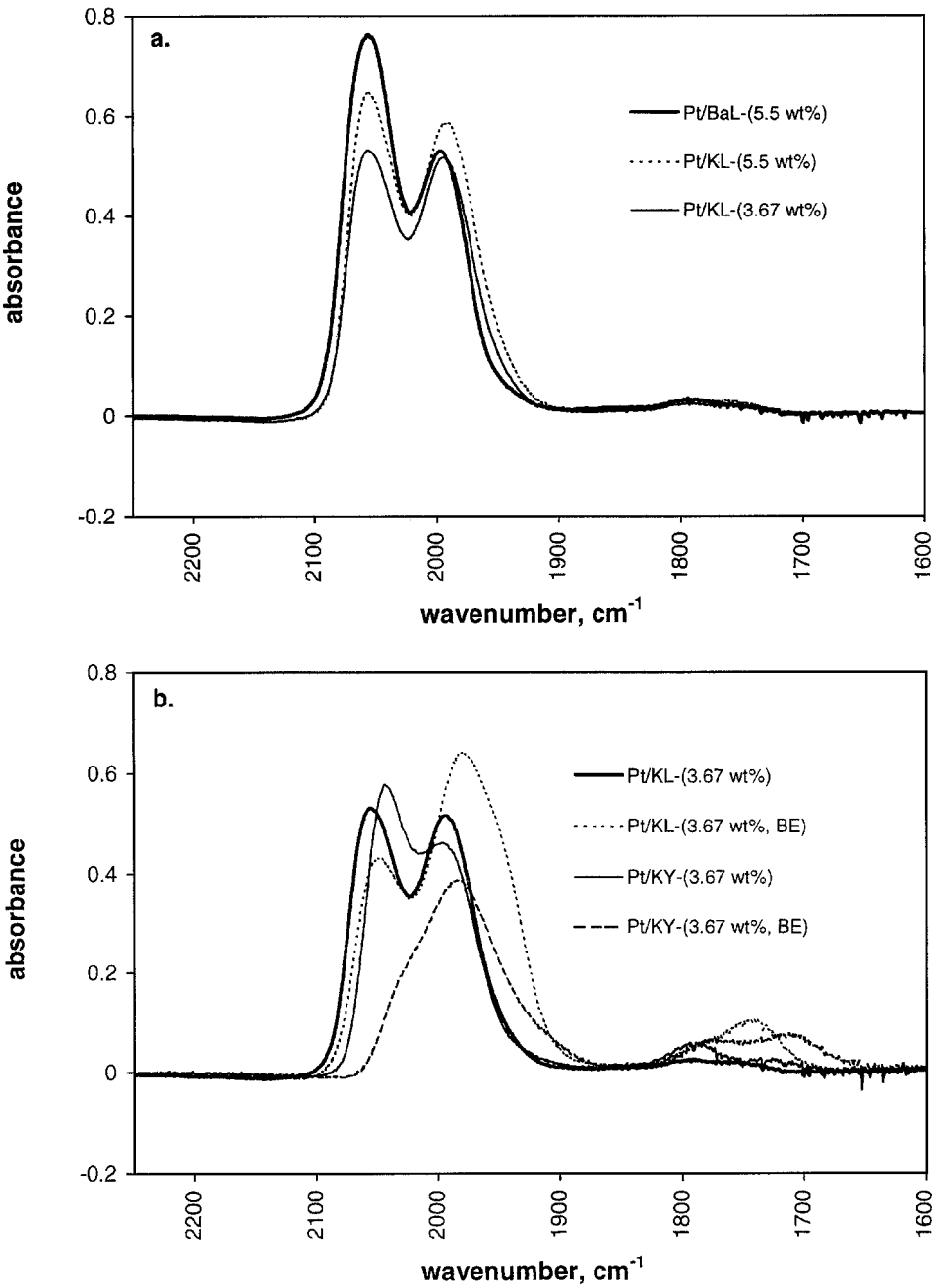

FIG. 2. Comparison of CO absorption spectra after equilibrating RT saturation uptakes of CO at 300°C in helium. a. 3.67 and 5.5 wt% Pt/L-zeolite samples. b. 3.67 wt% Pt/L-zeolite and Pt/Y-zeolite samples.

samples and about 6 for the 5.5 wt% Pt/BaK L-zeolite sample and the 3.67 wt% Pt/K Y-zeolite samples, consistent with the hydrogen chemisorption results (Table 1). Therefore, the coordinative unsaturation of the surface metal atoms in the Pt/Y-zeolite samples relative to the Pt/L-zeolite samples is not simply due to a particle size effect (since the 3.67 wt% Pt/L-zeolite samples are significantly smaller than the 5.5 wt% Pt/BaKL and the Pt/Y-zeolite samples), but instead due to a particle morphology effect, suggesting that the zeolite structure influences the specific morphology of the metal particles formed. A unique morphology effect was earlier observed in the XAFS analysis of palladium supported on K L-zeolite prepared in a similar manner (35), where the absence/near absence of the second coordination shell and the high Pd–O contributions suggested the formation of raft-like particles within the zeolite lattice. While for the Pt/L-zeolite samples, the morphology of the metal particles formed was different from that formed for the Pd/L-zeolite samples (since the second coordination shell was clearly present), a similar effect can be expected

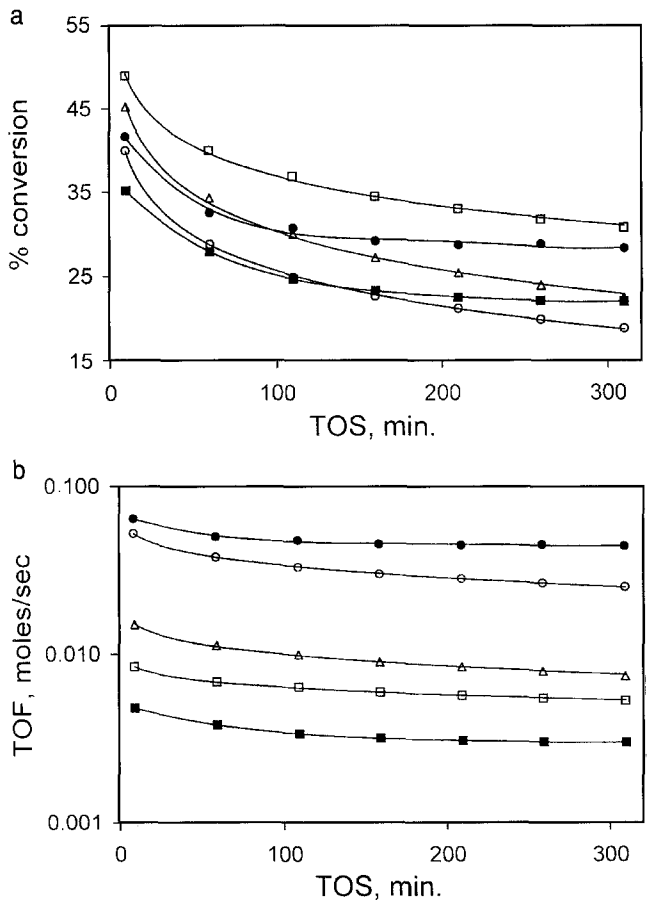

FIG. 3. Deactivation profiles for n-hexane conversion over the different catalysts. △, Pt/BaKL-(5.5 wt%); □, Pt/KL-(3.67 wt%); ■, Pt/KL-(3.67 wt%, BE); ○, Pt/KY-(3.67 wt%); ●, Pt/KY-(3.67 wt%, BE).

where the zeolite lattice structure directs the formation of metal particles of a specific morphology.

Deactivation of the Catalysts Samples during Reaction

The deactivation of the catalyst samples during reaction is shown in Fig. 3a. It is observed that under these reaction conditions all of the catalysts samples deactivate, with the extent of deactivation ranging between 50% of initial activity for the Pt/KY-(3.67 wt%) sample and 30% of initial activity for the Pt/KY-(3.67 wt%, BE) sample. This deactivation can be attributed to coking. From Figs. 4a–g (but not 4h) it can be seen that the selectivity to products remains almost unchanged after an initial transition period. This is consistent with there being two different mechanisms of deactivation. The initial transient period corresponds to a buildup of carbon atoms on the surface of the metal particles, which may be due to the low hydrogen partial pressure used in this study (0.16 atm) and which can have both an electronic and a geometric (ensemble) effect on product selectivities. In the latter period (after ~100 min TOS), the product selectivities remain almost unchanged with further deactivation, suggesting that this deactivation is caused by pore blockage. From Fig. 3a, it is observed that back-exchange of the Brønsted acidity results in considerably less deactivation caused by the latter mechanism of catalyst deactivation. Ostgard *et al.* (41) observed that Pt/L-zeolite samples prepared by impregnation deactivated less than Pt/L-zeolite samples prepared by ion-exchange (containing residual Brønsted acidity) during n-hexane conversion over these catalysts. These results suggest that the latter deactivation process requires the presence of Brønsted acidity. Lerner *et al.* (42) observed that for n-hexane conversion over Pt/Na-Mordenite and Pt/H-Mordenite catalysts, the coke formed on the Pt/Na-Mor sample was about one-third of that formed on the Pt/H-Mor sample and could be oxidized at lower temperatures in a subsequent temperature-programmed oxidation (TPO) study. They proposed that the coke associated with the acid sites leads to pore blockage (42), in agreement with our own observations.

The selectivity to hexenes increases with increasing TOS (Fig. 4h). However, as seen in Fig. 5, the hexenes/n-hexane ratio remains almost constant over the different catalysts. This suggests that under these reaction conditions, n-hexane dehydrogenation to hexenes is the only reaction which proceeds to thermodynamic equilibrium, while the remaining reactions are all kinetically controlled. As seen in Figs. 4e–f, the selectivity to 2MP, 3MP, and MCP remains almost unchanged with deactivation after the initial transient period. For these metal loadings, the Brønsted acidity is expected to be uniformly distributed throughout the zeolite channels, e.g., the 3.67 and 5.5 wt% Pt loadings in L-zeolite correspond to 1.8 and 2.7 protons per unit cell. Since it appears unlikely that the blockage of acid sites uniformly distributed along the zeolite channels will proceed at the same rate as the blockage of the metal particles (which are more discretely located), this indicates that the Brønsted acid sites generated in the ion-exchange procedure are catalytically inert under these reaction conditions. A similar conclusion was formed by Paal and co-workers for a Pt/NaY catalyst prepared by ion-exchange based on the analysis of the fragmentation products (12).

Electronic Effects and Effects of Particle Morphology on Catalyst Activity and Selectivity

The benzene selectivities for the different catalysts were observed to correlate with the electronic density of the metal particles, as measured by the CO stretching frequencies (Fig. 7). It was observed that the Pt/Y-zeolite samples have a higher activity and selectivity to benzene than the Pt/L-zeolite samples (Figs. 3a and 4g). This has also been observed by Paal and co-workers (12). The opposite trend was observed in the studies by Bernard (1) and Lane *et al.* (43). An explanation for this difference may lie in the method used to prepare the catalysts. Our samples, and those of Paal and coworkers (10, 12), were prepared by ion-exchange, while those used in the other studies were

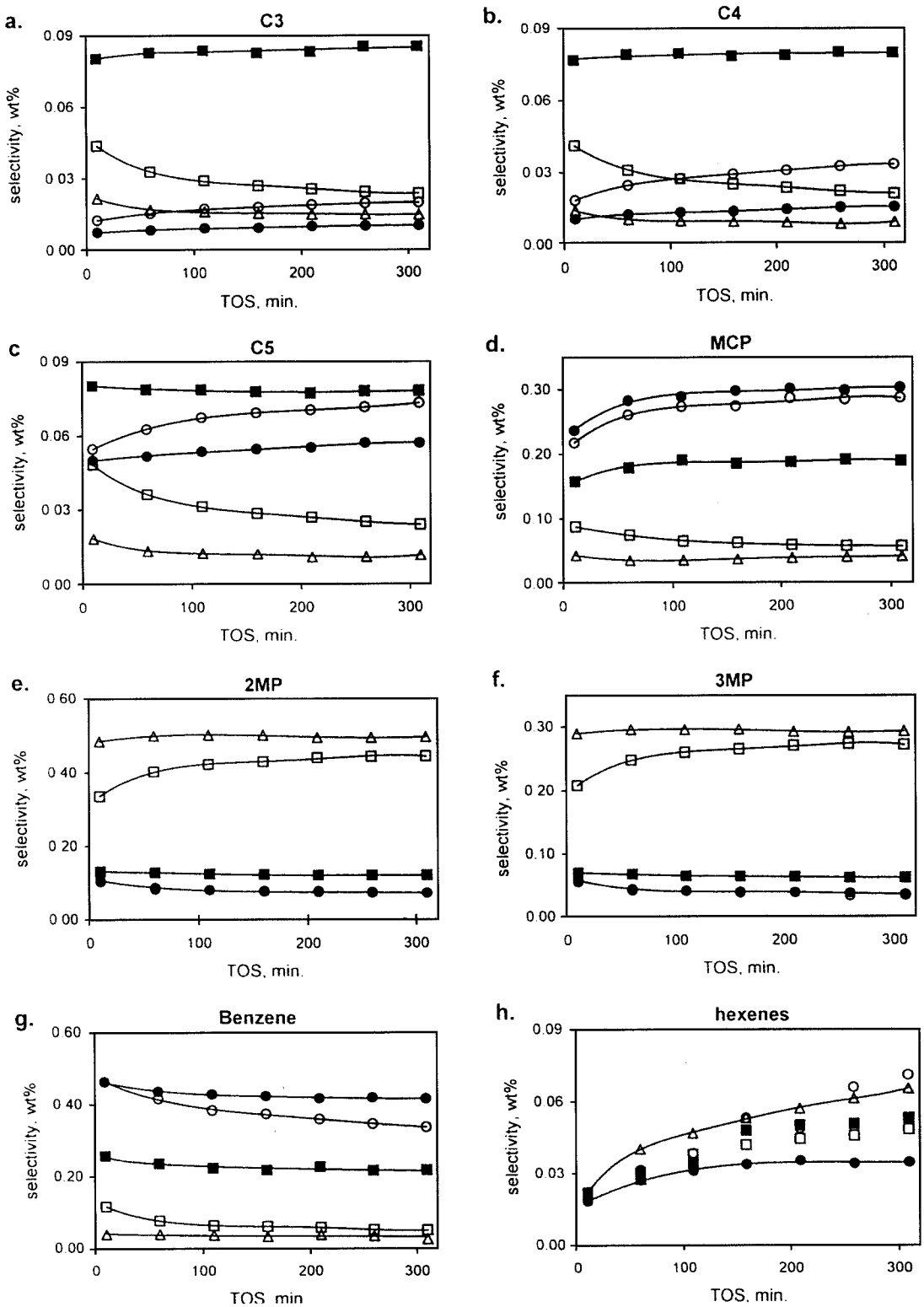

FIG. 4. Selectivity (wt%) to products vs time-on-stream (TOS). △, Pt/BaKL-(5.5 wt%); □, Pt/KL-(3.67 wt%); ■, Pt/KL-(3.67 wt%, BE); ○, Pt/KY-(3.67 wt%); ●, Pt/KY-(3.67 wt%, BE). Note: In Figs. 4e and 4f, ○ and ● are overlapped.

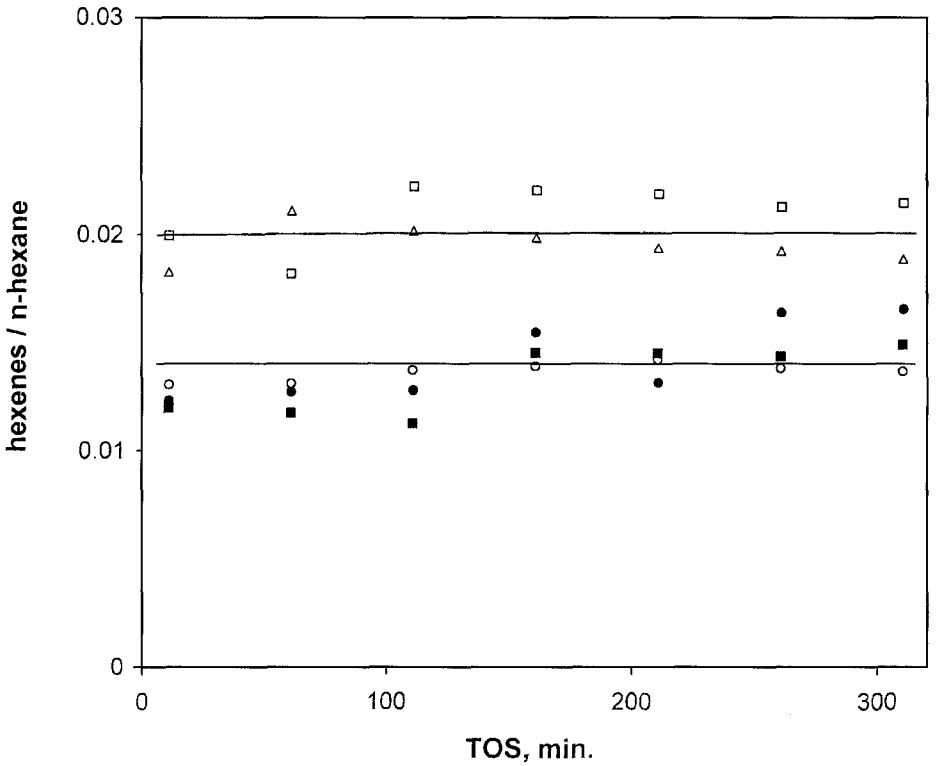

FIG. 5. Ratio of hexenes to n-hexane in product stream vs time-on-stream (TOS). △, Pt/BaKL-(5.5 wt%); □, Pt/KL-(3.67 wt%); ■, Pt/KL-(3.67 wt%, BE); ○, Pt/KY-(3.67 wt%); ●, Pt/KY-(3.67 wt%, BE).

prepared by impregnation (1, 43). It has been previously observed that these techniques give rise to different metal dispersions (41). For L-zeolite it was observed that impregnation of the metal precursor gives smaller metal particles compared to ion-exchange (41). This suggests an effect of the morphology of the metal particles formed. The observed lower activity of the Pt/L-zeolite samples compared to the Pt/Y-zeolite samples can also be due to a transport effect, because of slower diffusion of reactants (and products) in the unidimensional channels of L-zeolite. Since an increased residence time of the products in the zeolite channels can be expected to lead to increased secondary reactions, we checked the extent of secondary hydrogenolysis of 2MP and 3MP in the product stream for the different samples. Hydrogenolysis of 2MP and 3MP has been previously observed to predominantly form isobutane and isopentane (44, 45). Therefore, the ratio of the sum of isobutane and isopentane to the sum of isobutane, isopentane, 2MP and 3MP was taken as a measure of the extent of secondary reactions. The Pt/BaKL-(5.5 wt%) and Pt/KL-(3.67 wt%) samples had secondary hydrogenolysis conversions (i.e., (ib + ip)/(ib + ip + 2MP + 3MP)) of ~1%, the Pt/KL-(3.67 wt%, BE) had conversions of ~4%, and the Pt/KY-(3.67 wt%) and Pt/KY-(3.67 wt%, BE) had conversions of ~4 and 3%, respectively. Although no clear picture emerges from this comparison, one interesting observation is that for Pt/L-zeolite, back-exchange with K^+ increases the extent of secondary hydrogenolysis, while this effect is not observed for the Pt/Y-zeolite samples (where, in fact, less secondary hydrogenolysis is observed for the Pt/KY back-exchanged sample), suggesting that n-hexane conversion over the Pt/L-zeolite samples may be transport limited under these reaction conditions. This explanation is also consistent with the observation that the back-exchange of protons with K^+ leads to an increase in catalytic activity for the Pt/Y-zeolite samples (i.e., due to an electronic effect), but to a decrease in catalytic activity for the Pt/L-zeolite samples (i.e., due to a transport effect) and that the observed TOF for Pt/KY-(3.67 wt%, BE) is an order of magnitude greater than for the back-exchanged Pt/KL sample (see Fig. 3b). However, as can be seen from Fig. 4g, the benzene selectivity correlates with increasing electron density of the surface metal atoms (as indicated by the CO infrared stretching frequency), demonstrating that the selectivity is less affected by transport effects.

In previous studies, the propensity for terminal hydrogenolysis has been correlated with an increase in benzene selectivity (2, 4). From Figs. 4g and 6c, it is seen that the Pt/Y-zeolite samples which have the highest benzene selectivity also have the highest propensity for terminal hydrogenolysis. But an interesting observation is that the Pt/BaKL-(5.5 wt%), Pt/KL-(3.67 wt%), and Pt/KL-(3.67 wt%, BE) samples all have the same propensity for terminal hydrogenolysis (even though Pt/KL-(3.67 wt%,

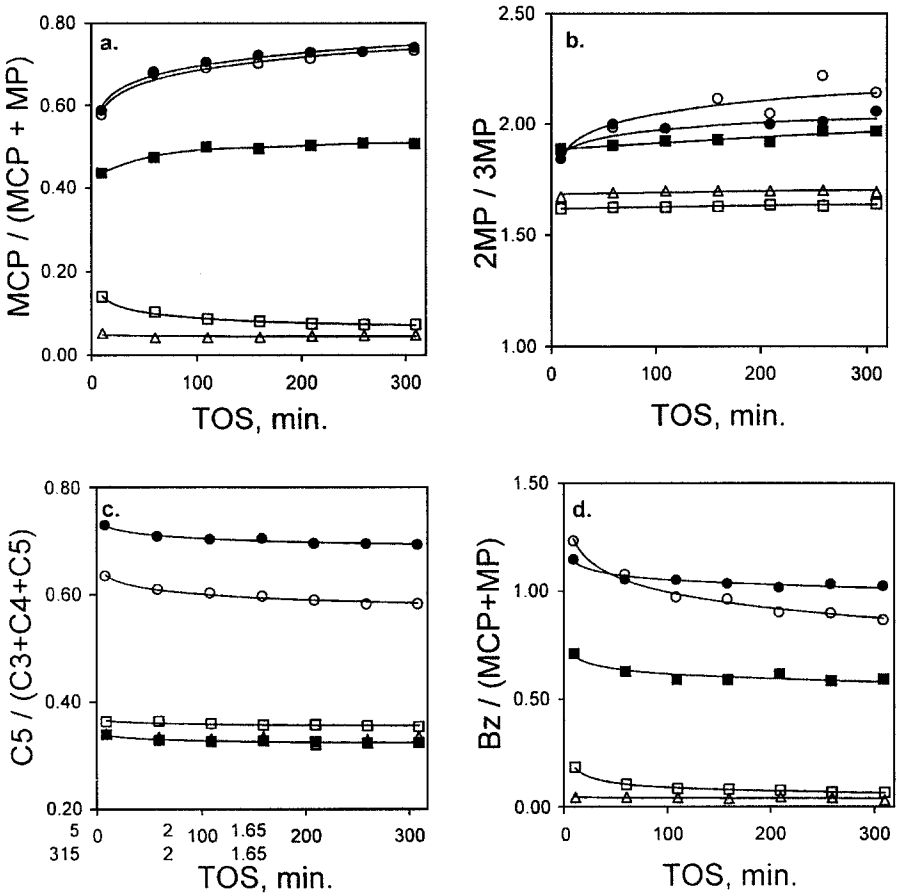

FIG. 6. Product distribution patterns vs time-on-stream (TOS). △, Pt/BaKL-(5.5 wt%); □, Pt/KL-(3.67 wt%); ■, Pt/KL-(3.67 wt%, BE); ○, Pt/KY-(3.67 wt%); ●, Pt/KY-(3.67 wt%, BE).

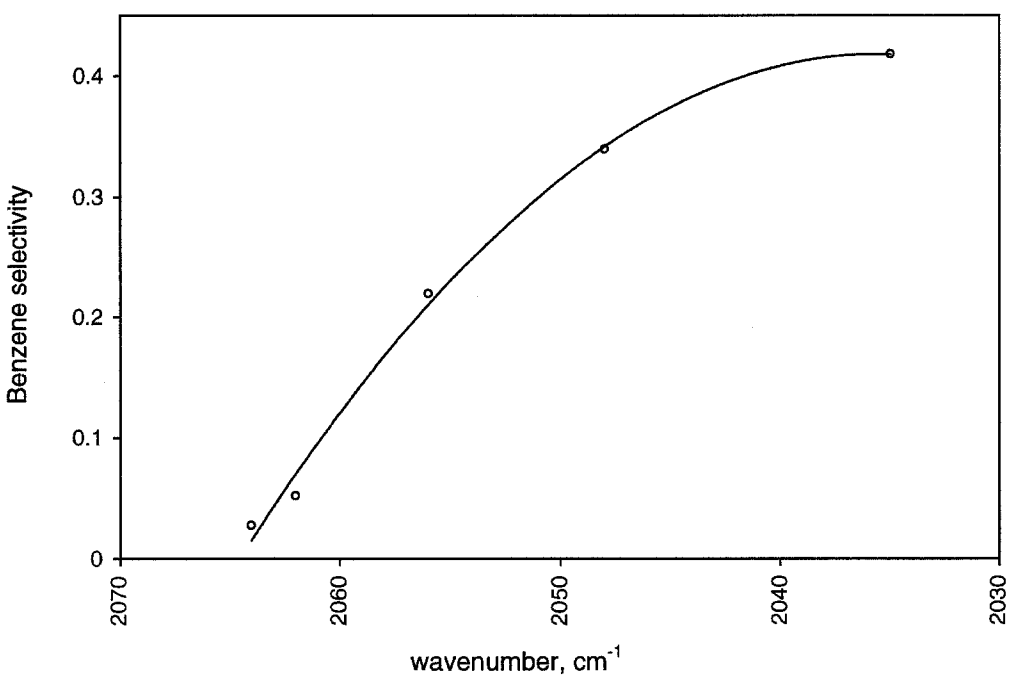

FIG. 7. Benzene selectivity (after 310 min TOS) vs stretching frequency of linearly adsorbed CO (after equilibration in helium at 300°C for 30 min).

BE) has a much higher benzene selectivity than the other two catalysts). As noted earlier, the Pt/BaKL-(5.5 wt%) and the Pt/KL-(3.67 wt%) samples have very similar CO absorption bands, suggesting that the CO adsorption sites are similar over these catalysts. Also, from the XAFS (33), the particle morphologies for the 3.67 wt% Pt/KL-zeolite samples (IE and BE) are the same. This indicates that the propensity for terminal hydrogenolysis is primarily determined by the morphology of the metal particles and the surface sites exposed for adsorption of the reactants.

Moretti and Sachtler (46) have proposed that the ratio of MCP ring opening products (i.e., the ratio of 2MP to 3MP) is related to a geometric effect. However, in the present study, the samples that display a higher electron density on the surface metal atoms (i.e., the Pt/KL-BE, the Pt/KY, and the Pt/KY-BE samples) had a 2MP to 3MP ratio close to the statistically expected value of 2, while the more electron deficient metal particles (the 5.5 wt% Pt/BaKL and the 3.67 wt% Pt/KL samples) had 2MP/3MP ratio of about 1.65. This suggests that the higher 2MP/3MP ratios correlate with an increased electron density of the metal particles. A similar conclusion was reached by Clarke *et al.* (47), who proposed that the high 2MP/3MP ratios (~3) observed over platinum supported on magnesia was due to a shift of negative charge from the magnesia O^{2-} ions to the platinum. The results of Moretti and Sachtler (46) are consistent also with this interpretation, as the lower 2MP/3MP ratios were observed over much larger metal particles.

Paal (13, 14) has suggested that the ratio of MCP to isomer products is a measure of the abundance of surface hydrogen under reaction conditions, with less hydrogen favoring more of the MCP product. From Figs. 4g and 6a, it can be seen that the higher the benzene selectivity, the higher is the MCP/(MCP + MP) ratio. The benzene selectivity decreases in the initial period of deactivation, probably due to an ensemble effect of the deposition of carbon atoms, while the MCP/(MCP + MP) ratio increases in this period, indicating surface hydrogen depletion. A comparison of the CO infrared results with benzene selectivity (Fig. 7) shows that the more electron rich the metal surface sites appeared, the higher was the benzene selectivity (and the MCP/(MCP + MP) ratio). This is consistent with previous studies of n-hexane conversion over monofunctional platinum catalysts (1, 11, 41). However, we would like to emphasize that this electronic effect can be caused either by a metal–support type interaction involving charge transfer between the metal particles and the support, or it can be related to the specific morphologies of the metal particles formed on different supports and on using different preparation methods. Therefore, the effect of the support in the high activity and aromatization selectivity of a monofunctional platinum catalyst for n-hexane conversion can be twofold, i.e., the stabilization of extremely small metal particles of specific morphology under reaction conditions and metal–support interaction resulting in an increased electron density over the metal particles.

CONCLUSIONS

n-Hexane conversion over zeolite-supported platinum catalysts has been studied at 360°C in a packed bed reactor. The observed activity and selectivity for n-hexane conversion over these catalysts is seen to be affected by factors such as the morphology of the metal particles, electronic perturbation of the metal particles and the transport of reactants and products within the zeolite channels. In the absence of sulfur impurities, the deactivation appears to be due to two types of coking. Initially, the effect of the deposition of carbon atoms on the surface of the metal particles can be observed, and further, deactivation is caused by pore blockage. The propensity for terminal hydrogenolysis is primarily determined by the particle morphology, i.e. the type of surface sites exposed. The increase in benzene selectivity correlates with a shift to lower stretching frequencies of the CO absorption bands, indicating that an increase in the electron density at the surface metal atoms results in higher benzene selectivity. This increase in electron density can be caused either by a metal–support interaction involving charge transfer between the metal particles and the support, or as a result of the particle morphology, depending on the coordination of the surface metal atoms. The effect of the support in the high activity and aromatization selectivity of a monofunctional platinum catalyst for n-hexane conversion can be twofold, i.e., the stabilization of extremely small metal particles of specific morphology under reaction conditions and metal–support interaction resulting in an increased electron density over the metal particles.

ACKNOWLEDGMENTS

This work was partially supported by a grant from NSF.

REFERENCES

1. Bernard, J. R., *in* "Proceedings, Fifth International Congress on Zeolites" (L. V. C. Rees, Ed.), p. 686. Heyden, London, 1980.
2a. Tauster, S. J., and Steger, J. J., *J. Mater. Res. Soc. Symp. Proc.* **111**, 419 (1988).
2b. Tauster, S. J., and Steger, J. J., *J. Catal.* **125**, 387 (1990).
3. Derouane, E. G., and Vanderveken, D. J., *Appl. Catal.* **45**, L15 (1988).
4. Mielczarski, E., Hong, S. B., Davis, R. J., and Davis, M. E., *J. Catal.* **134**, 359 (1992).
5. Iglesia, E., and Baumgartner, J. E., *in* "Proceedings, Tenth International Congress on Catalysis, Budapest 1992" (L. Guczi, F. Solymosi, and P. Tetenyi, Eds.), p. 157. Akademiai Kiado, Budapest, 1993.
6. Sharma, S. B., Ouraipryvan, P., Nair, H. A., Balaraman, P., Root, D. W., and Dumesic, J. A., *J. Catal.* **150**, 234 (1994).
7. Davis, R. J., and Derouane, E. G., *J. Catal.* **132**, 269 (1991).
8. Manninger, I., Xu, X. L., Tetenyi, P., and Paal, Z., *Appl. Catal.* **51**, L7 (1989).

9. Paal, Z., Zhan, Z., Manninger, I., and Muhler, M., *Appl. Catal.* **66**, 301 (1990).
10. Manninger, I., Zhan, Z., Xu, X. L., and Paal, Z., *J. Molec. Catal.* **66**, 223 (1991).
11. Zhan, Z., Manninger, I., Paal, Z., and Barthomuef, D., *J. Catal.* **147**, 333 (1994).
12. Paal, Z., Zhan, Z., Manninger, I., and Sachtler, W. M. H., *J. Catal.* **155**, 43 (1995).
13. Paal, Z., *in* "Hydrogen Effects in Catalysis" (Z. Paal and P. G. Menon, Eds.), p. 449. Dekker, New York, 1988.
14. Paal, Z., *J. Catal.* **156**, 301 (1995).
15. Sheppard, N., and Nguyen, T. T., *in* "Advances in Infrared and Raman Spectroscopy, Vol. 5" (R. G. H. Clark and R. E. Hester, Eds.), Chap. 2. Heyden, London, 1978.
16. Besoukhanova, C., Guidot, J., Barthomuef, D., Breysse, M., and Bernard, J. R., *J. Chem. Soc., Faraday Trans. I* **77**, 1595 (1981).
17. de Mallman, A., and Barthomuef, D., *Stud. Surf. Sci. Catal.* **46**, 429 (1989).
18. Larsen, G., and Haller, G. L., *Catal. Lett.* **3**, 103 (1989).
19. Kustov, L. H., Ostgard, D., and Sachtler, W. M. H., *Catal. Lett.* **9**, 121 (1991).
20. Han, W., Kooh, A. B., and Hicks, R. F., *Catal. Lett.* **18**, 193 (1993).
21. Lane, G. S., Miller, J. T., Modica, F. S., and Barr, M. K., *J. Catal.* **141**, 465 (1993).
22. Cotton, F. A., and Wilkinson, G., *in* "Advances in Inorganic Chemistry," p. 728, Wiley-Interscience, New York, 1967.
23. Sung, S., and Hoffman, R., *J. Amer. Chem. Soc.* **107**, 579 (1985).
24. van Santen, R. A., *J. Chem. Soc., Faraday Trans. I* **83**, 1915 (1987).
25. Menacherry, P. V., and Haller, G. L., *Catal. Lett.*, submitted.
26. Blyholder, G., *J. Phys. Chem.* **68**, 2772 (1964).
27. Greenler, R. G., Burch, K. D., Kretzschmar, K., Klauser, R., Bradshaw, A. M., and Hayden, B. E., *Surf. Sci.* **152/153**, 338 (1985).
28. van Hardeveld, R., and Hartog, F., *Surf. Sci.* **15**, 189 (1969).
29. Kappers, M. J., and van der Maas, J. H., *Catal. Lett.* **10**, 365 (1991).
30. Hammaker, R. M., Francis, S. A., and Eischens, R. P., *Spectrochim. Acta* **21**, 1295 (1965).
31. Hollins, P., and Pritchard, J., *Progr. Surf. Sci.* **19**, 275 (1985).
32. Hollins, P., *Surf. Sci. Rep.* **16**, 51 (1992).
33. Menacherry, P. V., and Haller, G. L., *J. Catal.* **167**, 425 (1997).
34. Menacherry, P. V., Ph.D. thesis, Yale University, 1997.
35. Menacherry, P. V., Fernandez-Garcia, M., and Haller, G. L., *J. Catal.* **166**, 75 (1997).
36. Press, W. H., Teukolsky, S. A., Vetterling, W. T., and Flannery, B. P., "Numerical Recipes in C," 2nd ed., p. 645. Cambridge Univ. Press, London, 1992.
37. Vaarkamp, M., Miller, J. T., Modica, F. S., Lane, G. S., and Koningsberger, D. C., *J. Catal.* **138**, 675 (1992).
38. McVicker, G. B., Lao, J. K., Ziemak, J. J., Gates, W. E., Robbins, J. L., Treacy, M. M., Rice, S. B., Vanderspurt, T. H., Cross, V. R., and Ghosh, A. K., *J. Catal.* **139**, 48 (1993).
39. Dalla Beta, R. A., and Boudart, M., *in* "Proceedings, Fifth International Congress on Catalysis, Palm Beach, 1972" (J. W. Hightower, Ed.), p. 1329. North-Holland, Amsterdam, 1973.
40. Gallezot, P., *Catal. Rev. Sci. Eng.* **20**(1), 121 (1969).
41. Ostgard, D. J., Kustov, L., Poeppelmeier, K. R., and Sachtler, W. M. H., *J. Catal.* **133**, 342 (1992).
42. Lerner, B. A., Carvill, B. T., and Sachtler, W. M. H., *Catal. Today* **21**, 23 (1994).
43. Lane, G. S., Modica, F. S., and Miller, J. T., *J. Catal.* **129**, 145 (1991).
44. Leclercq, G., Leclerq, L., and Maurel, R., *J. Catal.* **50**, 87 (1977).
45. Garin, F., Aeiyach, S., Legare, P., and Maire, G., *J. Catal.* **77**, 323 (1982).
46. Moretti, G., and Sachtler, W. M. H., *J. Catal.* **116**, 350 (1989).
47. Clarke, J. K. A., Bradley, M. J., Garvie, L. A. J., Craven, A. J., and Baird, Ti., *J. Catal.* **143**, 122 (1993).